Nonlinear Light Scattering and Spectroscopy of Particles and Droplets in Liquids

Sylvie Roke[1,2] and Grazia Gonella[3]

[1]Laboratory for fundamental BioPhotonics (LBP), Institute of Bioengineering (IBI), School of Engineering, École Polytechnique Fédérale de Lausanne (EPFL), 1015 Lausanne, Switzerland; email: sylvie.roke@epfl.ch

[2]Max-Planck Institute for Metals Research, 70569 Stuttgart, Germany

[3]Department of Chemistry, Temple University, Philadelphia, Pennsylvania 19122; email: gonella@temple.edu

Annu. Rev. Phys. Chem. 2012. 63:353–78

First published online as a Review in Advance on January 17, 2012

The *Annual Review of Physical Chemistry* is online at physchem.annualreviews.org

This article's doi: 10.1146/annurev-physchem-032511-143748

0066-426X/12/0505-0353$20.00

Keywords

second harmonic generation, sum frequency generation, hyper-Rayleigh scattering, vesicles, micelles, emulsions, cells

Abstract

Nano- and microparticles have optical, structural, and chemical properties that differ from both their building blocks and the bulk materials themselves. These different physical and chemical properties are induced by the high surface-to-volume ratio. As a logical consequence, to understand the properties of nano- and microparticles, it is of fundamental importance to characterize the particle surfaces and their interactions with the surrounding medium. Recent developments of nonlinear light scattering techniques have resulted in a deeper insight of the underlying light-matter interactions. They have shed new light on the molecular mechanism of surface kinetics in solution, properties of interfacial water in contact with hydrophilic and hydrophobic particles and droplets, molecular orientation distribution of molecules at particle surfaces in solution, interfacial structure of surfactants at droplet interfaces, acid-base chemistry on particles in solution, and vesicle structure and transport properties.

1. INTRODUCTION

SFG: sum frequency generation

SHG: second harmonic generation

NLS: nonlinear light scattering

HRS: hyper-Rayleigh scattering

λ: wavelength

MG: malachite green

PS: polystyrene

Nanoparticles, microparticles, and droplets have found application in a broad range of fields, spanning from medicine, pharmacy, and biotechnology to the paint industry, electronics, optics, and the environment. Nanoparticles and microparticles have optical, structural, and chemical properties that are significantly altered from both their constituents (atoms or molecules) and the bulk materials themselves. This difference is size induced and results from the large surface-to-volume ratio. Therefore, to understand the properties of nanoparticles and microparticles, it is of fundamental importance to characterize the particle surfaces and the interaction of the surface with the surrounding medium. Similarly, small droplets or particles dispersed in a bulk medium can be unique tools to study liquid/liquid, solid/solid, solid/liquid, gas/solid, or gas/liquid interfaces.

Because of their fundamental and technological importance, nanoparticles have been the focus of intense research in many fields, one of which is nonlinear optics. Second-order nonlinear optical techniques are particularly sensitive to interface properties because such processes are forbidden (under the electric dipole approximation) in centrosymmetric media. However, traditional nonlinear optical methods in transmission or reflection geometry, such as sum frequency generation (SFG) and second harmonic generation (SHG), are difficult to apply to interface studies in situ owing to the intrinsic turbid nature of a sample that contains particles, droplets, or grains. Nonlinear light scattering (NLS) methods, however, utilize these effects and can therefore be used to probe the nonlinear optical and interfacial properties of small particles and droplets in liquids.

NLS is a combination of nonlinear optics and light scattering. The first report of such a process dates from 1965, when Terhune et al. (1) reported that when a beam of a ruby laser is focused in water or quartz, scattered light at the double frequency can be detected. The light originates from the focal region and its intensity depends quadratically on the incoming laser intensity. In this experiment, signal was detected at 90° with respect to the incoming laser beam and at both the second harmonic (SH) frequency (elastic scattering) and frequencies with a displacement of one vibrational transition from the SH frequency (inelastic scattering).

Light scattering occurs when photons encounter impurities or inhomogeneities. Such impurities can consist of density fluctuations, molecules, or particles. The observation that SHG could occur in a centrosymmetric medium in a non-phase-matched direction was explained by noting that on the molecular time and length scale, there are local density fluctuations in any medium: The incoming laser beam generates a small dipole contribution in every molecule. On average, in an isotropic material, these contributions vanish, but when enough photons are present, a small residual signal resulting from the fluctuations in the distribution in the medium remains. Nonlinear elastic and inelastic light scattering have been termed hyper-Rayleigh scattering (HRS) and hyper-Raman scattering, respectively (2). The intensity in both types of scattering depends linearly on the number of source molecules as it is incoherent scattering.

When the size of the inhomogeneity becomes an appreciable fraction of the scattered wavelength (λ_{SF}), detectable coherent effects begin to emerge. NLS from particles with sizes $\sim\lambda_{SF}/50$ can already display the effects of correlated emission (coherence). These coherent processes can originate from either the surface of the particles or the bulk.

The use of a nonlinear, second-order scattering process to obtain information about surface chemistry of particles in liquids was demonstrated in 1996 by the Eisenthal group (3). They reported the emission of SH signal from malachite green (MG) adsorbed to the surface of micron-sized centrosymmetric polystyrene (PS) particles. The SH scattered intensity was observed to depend linearly on the number of particles in solution and quadratically on the MG concentration.

The quadratic dependence proves that the signal that originates from MG molecules adsorbed on the surface of each particle adds up coherently, whereas the linear dependence proves that the signal from different particles adds up incoherently.

Vibrational sum frequency scattering (SFS) was demonstrated seven years later (4) and can also be used to probe the interfacial properties of particles in liquid and solid media. The difference with second harmonic scattering (SHS) is that the incoming beams are of different frequency, and one of the frequencies can be tuned to the energy of vibrational transitions. The resulting effect is that the vibrational spectrum of a molecular layer with a thickness of typically one to two molecular dimensions at the particle interface can be measured.

SFS: sum frequency scattering

SHS: second harmonic scattering

k: wave vector

E: electric field

The aim of this review is to give an introduction to NLS methods and to discuss recent advances in the field. More specifically, the connecting framework between the different methods is presented. **Figure 1** displays objects of different sizes that have been or could be studied with NLS: molecules, micelles, nanoparticles, vesicles, droplets (emulsions), cells. The size of the object with respect to the wavelength in combination with the type of light-matter interaction determines the dominant scattering process. For excitation with visible light, typically parametric light scattering, such as HRS and hyper-Raman scattering, occurs for objects <10 nm; SHS, SFS, and random quasi phase matching occur for objects <20 μm. Larger objects produce reflected or refracted beams, which can be measured with SHG or SFG in reflection or transmission

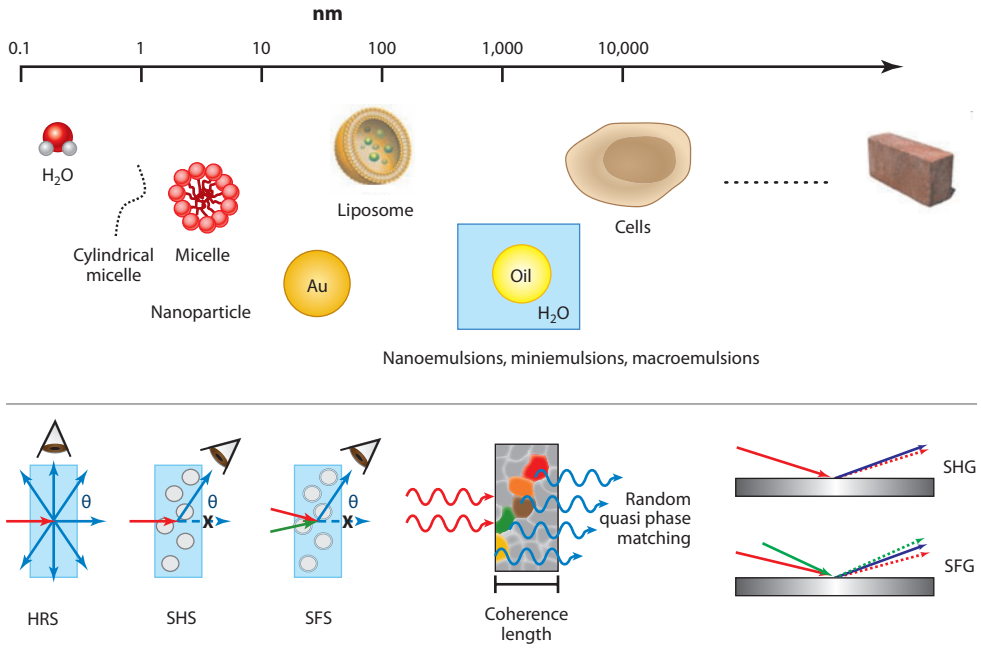

Figure 1

Display of objects, from small to large, from which light can induce nonlinear light scattering phenomena: molecules, micelles, nanoparticles, vesicles, droplets (emulsions), and cells. For excitation with visible light, HRS and hyper-Raman scattering typically occur for objects <10 nm; SHS, SFS, and random quasi phase matching occur for objects <20 μm. Larger objects produce reflected or refracted beams, which can be measured with SHG and SFG in reflection or transmission mode. Abbreviations: HRS, hyper-Rayleigh scattering; SFG, sum frequency generation; SFS, sum frequency scattering; SHG, second harmonic generation; SHS, second harmonic scattering.

mode. In Section 2, we give an overview of the fundamentals behind nonlinear light scattering. Section 3 is devoted to a description of experimental parameters. Section 4 picks up where Section 2 stopped, discussing the models and studies done to understand the optical properties of nanoparticles and microparticles. In Section 5, we discuss recent studies to understand the interfacial chemistry found in solution, and Section 6 offers a short introduction to biologically relevant topics. Finally, we end with conclusions and outlook. Due to space constraints, we do not treat all topics in depth. We focus our attention on offering an introduction aimed at pointing out the cohesion between the different studies, and we confine ourselves mostly to work done in liquid media. Recently, three reviews have appeared: one by Eisenthal (5) discussing the topic of the SHS of nanoparticles, microparticles, and liposomes in water; one by Ray (6) discussing the nonlinear optical properties of nanoparticles with a focus on HRS; and one by Brevet (7) on SHG in nanostructures.

2. FUNDAMENTAL CONCEPTS OF NONLINEAR LIGHT SCATTERING

In this section, we describe the fundamentals needed to understand the principles of NLS. We use the generalized case for light scattering from a particle induced by two beams having wave vectors $\mathbf{k}_1$ and $\mathbf{k}_2$. Where necessary we consider plane waves of the form $\mathbf{E}_i = \mathbf{E}_0 e^{-i\omega_i t} e^{-i\mathbf{k}_i \cdot \mathbf{r}}$. The beam waist is always much bigger than the particle. **Figure 2** shows a representative geometry, where the two incoming beams lie in the same (horizontal) plane as the outgoing scattered beam.

2.1. Sources of Light Scattering

For light scattering to occur, a discontinuity or an object for a photon to scatter on must be present. An electromagnetic field **E** that interacts with a molecule can induce a molecular dipole **p** of the form (2, 8)

$$\mathbf{p} = \boldsymbol{\alpha}^{(1)} \cdot \mathbf{E} + \frac{1}{2}\boldsymbol{\beta}^{(2)} : \mathbf{EE} + \frac{1}{6}\boldsymbol{\beta}^{(3)} : \mathbf{EEE} + \cdots, \quad (1)$$

where $\boldsymbol{\alpha}$ is the first-order polarizability, $\boldsymbol{\beta}^{(2)}$ the second-order polarizability (or first-order hyperpolarizability), and $\boldsymbol{\beta}^{(3)}$ the third-order polarizability. Each of these terms can act as a source for scattering. Equation 1 reflects the possibility that one or more interactions of an electric field with

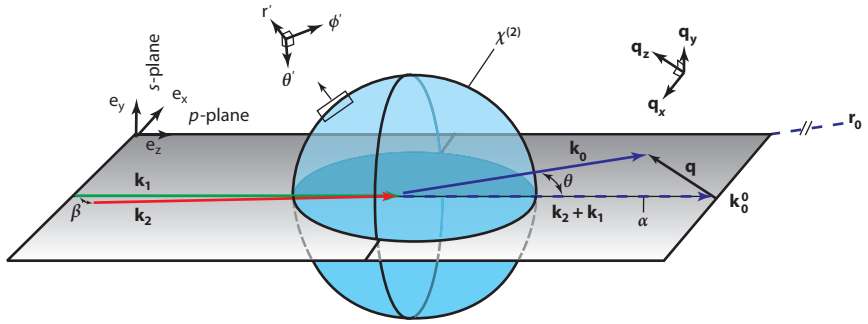

Figure 2

In-plane scattering geometry for nonlinear light scattering experiments, indicating the k-vectors of the incoming beams ($\mathbf{k}_1$ and $\mathbf{k}_2$) and the scattered sum frequency beam ($\mathbf{k}_0$), scattering wave vector (q), and in-plane scattering angle (θ). β is the angle between $\mathbf{k}_2$ and $\mathbf{k}_1$, and α is the angle between $\mathbf{k}_2$ and $\mathbf{k}_1 + \mathbf{k}_2 = \mathbf{k}_0^0$. $\mathbf{k}_0^0$ lies along the z-axis. Beams polarized parallel to the plane of incidence are defined as p-polarized, whereas beams with an oscillating field in the y-direction are indicated as s-polarized. The direction $\mathbf{k}_1 + \mathbf{k}_2$ is called the forward direction ($\theta = 0$).

a molecule might generate a dipole that oscillates at one of the fundamental frequencies, the sum or the difference of those frequencies. Such an oscillation consists of charges that accelerate and decelerate, which means that they can emit photons. In theoretical models, it is useful to describe such oscillating charges as currents that can be either bound (to a molecule/dielectric) or free (in a metal). In both cases, the current density $\mathbf{j}$ is given by: $\mathbf{j} = d\mathbf{P}/dt$. For an introduction to the physics behind emission of light from a dipole, the Feynman lectures (9, ch. 28) offer an insightful equation-free description. A more thorough mathematical derivation can be found in Reference 10 (ch. 9) or in Reference 11 (ch. 15). A book by Long (12) offers a recent and in-depth treatment of Raman scattering.

β: hyperpolarizability tensor

χ: susceptibility tensor

Starting with the first term, linear scattering already occurs at low light intensities. An example of this $\boldsymbol{\alpha}$-induced scattering is Rayleigh scattering as seen from the sky. In this case, the dipoles of the molecules in the atmosphere are the source of the scattered sunlight. Other forms of linear light scattering are fluorescence and Raman scattering; these are inelastic forms of scattering and depend on the transition moments of the molecules.

2.2. Incoherent Nonlinear Light Scattering

NLS occurs only at much higher field strengths, which is why it was only observed shortly after the invention of the laser. For such light scattering, the induced dipole depends at least quadratically on the field strength of the incoming beams. $\boldsymbol{\beta}$-induced light scattering can be HRS, hyper-Raman scattering, or two-photon fluorescence. As with linear light scattering, the $\boldsymbol{\beta}$ tensor is different for each form and represents the symmetry properties and energy states of the molecules. For a general three-photon scattering process arising from randomly oriented noncorrelated molecules, the measured intensity (I) can be expressed in the form

$$I(\omega_1 + \omega_2) = GN\langle\beta^{(2)}_{ijk}\beta^{*(2)}_{lmn}\rangle I(\omega_1)I(\omega_2), \tag{2}$$

where G includes physical constants and experimental factors and N is the molecular concentration (13). The relationship between $\langle\beta^{(2)}_{ijk}\beta^{*(2)}_{lmn}\rangle$ and the molecular tensor components β_{ijk} depends on the polarization state of fundamental and SH light, the scattering geometry, and the molecular symmetry (1, 14–17). The brackets denote time averaging. Various schemes have been developed in order to distinguish between HRS and two-photon fluorescence, such as spectral separation (18), direct temporal separation (19), and temporal separation in the Fourier domain (20). Polarization dependencies of the parametric light scattering (21) and HRS (22, 23) measurements have been demonstrated previously.

2.3. From Point Dipole to Extended Object

Although molecules and very small particles can be considered as point dipoles characterized by $\boldsymbol{\alpha}$ or $\boldsymbol{\beta}$, as their size increases and they become an extended molecular structure or particle whose size is of the order of ~10 nm or larger, their response is represented by the sum of all molecular polarizations p. The total polarization (P) will therefore be

$$\mathbf{P}^{(1)} \sim N\langle\mathbf{p}^{(1)}\rangle, \tag{3a}$$

$$\mathbf{P}^{(2)} \sim N\langle\mathbf{p}^{(2)}\rangle, \tag{3b}$$

$$\mathbf{P}^{(3)} \sim N\langle\mathbf{p}^{(3)}\rangle. \tag{3c}$$

$P^{(2)}$: second-order polarization source

R: particle/droplet radius or effective radius

For linear light scattering of particles, it is the first-order susceptibility ($\mathbf{X}^{(1)}$) that forms the source of the light scattering. Similarly for NLS, the second-order ($\mathbf{X}^{(2)}$) or third-order ($\mathbf{X}^{(3)}$) susceptibility is relevant.

Within the dipole approximation, second-order nonlinear optical effects occur only in noncentrosymmetric media, so that they are restricted to crystals and crystallites with a noncentrosymmetric space group and to other regions where centrosymmetry is broken on the molecular length scale. As centrosymmetry is broken at interfaces, second-order techniques such as SHG and SFG can be used to probe interfaces of isotropic media. In such experiments, there is often a phase relationship between the individually excited dipoles, e.g., if they are present on the same surface. These techniques are therefore coherent techniques. Second-order nonlinear optical techniques have been used for decades to measure interfacial properties. The first observation of surface SHG of a molecular monolayer was made in 1969 by Brown & Matsuoka (24). Surface-specific SFG of a molecular monolayer was observed for the first time in 1987 by Guyot-Sionnest et al. (25) and Harris et al. (26). Both techniques rely on the same principles, with the difference that the transition moments for SHG that make up $\boldsymbol{\beta}^{(2)}$ are of an electronic nature, whereas for SFG a combined electronic/infrared transition is often utilized so that a simultaneous infrared and Raman transition is required. Many review articles on the use of these techniques exist; see, e.g., Reference 27 for a list of references on these methods. The third-order processes are allowed in centrosymmetric materials even in the dipole approximation so that they can be used to measure bulk properties.

2.4. Coherent Nonlinear Light Scattering

Using the susceptibility as a source term, the corresponding source polarizations at a point $\mathbf{r}'$ on a particle become (excluding nonlocal effects)

$$P_i^{(1)}(\mathbf{r}') = \chi_{ij}^{(1)}(\mathbf{r}')E_j(\mathbf{r}'), \tag{4a}$$

$$P_i^{(2)}(\mathbf{r}') = \chi_{ijk}^{(2)}(\mathbf{r}')E_j(\mathbf{r}')E_k(\mathbf{r}'), \tag{4b}$$

$$P_i^{(3)}(\mathbf{r}') = \chi_{ijkl}^{(3)}(\mathbf{r}')E_j(\mathbf{r}')E_k(\mathbf{r}')E_l(\mathbf{r}'). \tag{4c}$$

To distinguish between bulk-allowed and surface-specific SHG or SFG, the susceptibility tensor can be written as the sum of a bulk and a surface term. We touch upon this in Section 4.

When scattering occurs from a particle, the source polarizations $P_i^{(1)}(\mathbf{r}')$, $P_i^{(2)}(\mathbf{r}')$, or $P_i^{(3)}(\mathbf{r}')$ created at the different positions ($\mathbf{r}'$) on the particle need to be added together. We first describe (linear) light scattering from two points on a sphere with radius R, $\mathbf{r}'_1$, and $\mathbf{r}'_2$. An illustration is presented in **Figure 3**.

The incident field arriving at each point induces a source polarization: $\mathbf{P}(\mathbf{r}'_1)$ and $\mathbf{P}(\mathbf{r}'_2)$. At the detector position, the emitted fields have the phase factors $e^{-i\mathbf{k}_0\cdot(\mathbf{r}_0-\mathbf{r}'_1)}$ and $e^{-i\mathbf{k}_0\cdot(\mathbf{r}_0-\mathbf{r}'_2)}$. The difference in phase between the emitted beams at the detection plane P is $(\mathbf{k}_0 - \mathbf{k})(\mathbf{r}'_2 - \mathbf{r}'_1) = \mathbf{q}(\mathbf{r}'_2 - \mathbf{r}'_1)$. In a scattering process from a particle, the above description must be carried out over the entire bulk or surface of the particle so that the total response is an integration of the source polarization over all points of the particle. At the detector position, the emitted field components interfere and this results in the final scattered field.

q is called the scattering wave vector and plays a central role in all light scattering processes. An illustration of this process is given in **Figure 2**. For NLS of two beams with different frequency,

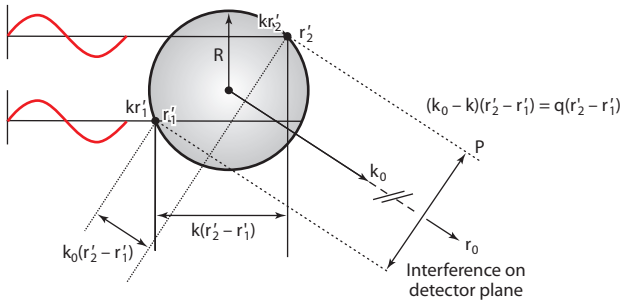

Figure 3

Light scattering. An incoming laser beam interacts with a particle. The path length difference that gives rise to scattering is illustrated for two points on a sphere. **k** is the wave vector of the incoming beams, and $\mathbf{k}_0$ is the wave vector of the scattered light.

$\mathbf{q} \equiv \mathbf{k}_0 - (\mathbf{k}_1 + \mathbf{k}_2)$, so that for negligible dispersion

$$q(\theta) = |\mathbf{q}| = 2|\mathbf{k}_0| \sin(\theta/2), \tag{5}$$

where $\mathbf{k}_0$ is the wave vector of the scattered field. The product of the magnitude of scattering wavevector and the radius of the particle qR is a measure of the phase mismatch encountered in a scattering process. At $\theta = 180°$, $qR = 2k_0R$. The product k_0R indicates the phase shift induced in the SH or sum frequency (SF) wave when it travels the distance of the particle radius. This is an important parameter for the theory as it states the extent to which the particle is subjected to a constant E-field. The resulting emitted field therefore depends on the size, shape, refractive index (at each wavelength), and structure of the particle and on the configuration of the incoming and outgoing beams.

To capture the symmetry properties of the scatterer and the beam geometry corresponding to the effective susceptibility for planar surfaces, the effective particle susceptibility was introduced (28). $\mathbf{\Gamma}$ captures the response of the particle, so that the scattered electric field for each of the process in Equation 4 becomes

$$E_i \propto E_j \frac{e^{ik_0r_0}}{r_0} \hat{\mathbf{i}} \cdot \Gamma^{(1)}_{ij}(f(\theta, \phi, R), \boldsymbol{\chi}^{(1)}) \cdot \hat{\mathbf{j}}, \tag{6a}$$

$$E_i \propto E_{1j} E_{2k} \frac{e^{ik_0r_0}}{r_0} \hat{\mathbf{i}} \cdot \Gamma^{(2)}_{ijk}(F(\theta, \phi, R), \boldsymbol{\chi}^{(2)}) : \hat{\mathbf{j}}\hat{\mathbf{k}}, \tag{6b}$$

$$E_i \propto E_{1j} E_{2k} E_{3l} \frac{e^{ik_0r_0}}{r_0} \hat{\mathbf{i}} \cdot \Gamma^{(3)}_{ijkl}(\mathcal{F}(\theta, \phi, R), \boldsymbol{\chi}^{(3)}) : \hat{\mathbf{j}}\hat{\mathbf{k}}\hat{\mathbf{l}}, \tag{6c}$$

where r_0 is the particle-detector distance; $f, F, \mathcal{F}$ are the form factors (usually Bessel-type functions) that depend on scattering angles θ (in-plane angle) and ϕ (out-of-plane angle); R is the particle radius; and $\hat{\mathbf{i}}, \hat{\mathbf{j}}, \hat{\mathbf{k}}, \hat{\mathbf{l}}$ are the unit vectors of the electric field polarization states (28, 29). Note that for light scattering of different orders, there are multiple form factors (30). If the detector position is far away, $|\mathbf{r}_0| \gg R$, as is usually the case in light scattering experiments, then the scattered light always appears at the detector as a spherical plane wave, i.e., $e^{ik_0r_0}/r_0$. This is called the far-field approximation.

Finally, for the emitted intensities we obtain

$$I \propto \frac{1}{r_0^2} I_1 |\mathbf{\Gamma}^{(1)}[f(\theta, \phi, R), \boldsymbol{\chi}^{(1)}]|^2, \tag{7a}$$

q: scattering wave vector

θ: in-plane scattering angle

$\mathbf{\Gamma}$: effective susceptibility tensor

$$I \propto \frac{1}{r_0^2} I_1 I_2 |\mathbf{\Gamma}^{(2)}[F(\theta, \phi, R), \boldsymbol{\chi}^{(2)}]|^2, \tag{7b}$$

$$I \propto \frac{1}{r_0^2} I_1 I_2 I_3 |\mathbf{\Gamma}^{(3)}[\mathcal{F}(\theta, \phi, R), \boldsymbol{\chi}^{(3)}]|^2. \tag{7c}$$

For the specific case of SFS, where vibrational resonances are probed and the signal is spectrally dispersed, the frequency dependence of the signal can be viewed as a scattering pattern arising from each probed vibrational mode. For the case of vibrational modes in combination with a weakly frequency dependent background, Equation 7*b* becomes in the frequency domain

$$I_{SFS}(\omega, \theta) \propto \left| \sum_n \left(A_{NR} h(\omega, \theta) e^{i\Delta\phi} + \frac{A_n(\theta)}{(\omega - \omega_{0n}) + i\Upsilon_n} \right) \right|^2, \tag{8}$$

where A_{NR} is the amplitude of a weakly dispersive background, $h(\omega, \theta)$ the spectral shape of the weakly dispersive background, n a vibrational mode with resonance frequency ω_{0n}, $A_n(\theta)$ the angle-dependent amplitude, Υ_n the half-width at half-maximum of vibrational mode n, and $\Delta\phi$ the phase difference between the resonant and weakly dispersive background signal. Note there is no relation between the scattering angle ϕ and the phase difference $\Delta\phi$. Thus, a wealth of information is available about the chemical interaction at the interface of a particle in a liquid. Section 5 shows an example.

2.5. Distinction Between Hyper-Rayleigh Scattering and Coherent Second Harmonic Scattering

A relatively large number of studies (e.g., 6, 31–51) has used the term HRS scattering for NLS from particles with $R > \lambda_{SF}/50$. In such cases, the use of the term HRS refers to the fact that the SH signal is measured in the classical HRS experimental configuration (**Figure 4*b***) and that the signal from the different scattering sources adds up incoherently, even though the signal is generated coherently from each scatterer. Based on the underlying physical principles, the use of the term HRS should really be restricted to point sources, i.e., for visible light, objects no larger than 5–10 nm. The reasoning is as follows: Linear Rayleigh scattering is defined as incoherent scattering from (dipole) point sources, e.g., $R \ll \lambda$ (52). Therefore, the light-matter interaction can be described by the first term of Equation 1. For HRS, in analogy, the second term of Equation 1 should hold. Deviations from Equation 1 start to occur as soon as the amplitude and the phase of the **E** field are changed by the particle. This results in coherent surface effects and bulk dispersive terms that are summarized in Section 4 (Equation 10). For scattering from metallic particles, a useful parameter is the skin depth, which is in the order of 5–10 nm for visible light. It is therefore logically consistent to refer to SHS that originates from objects below 5–10 nm as HRS, especially when the shape is not spherical. For larger objects, the term is no longer appropriate.

3. EXPERIMENTAL CONSIDERATIONS

For SHS and SFS, we have the following equation for the number of photons generated in a slab of the laser focus (N_{ph}):

$$N_{ph} \propto |\Gamma^{(2)}|^2 I_2 I_1 A \tau_p f S_{det}, \tag{9}$$

where I_i is the intensity of the beams, $\Gamma^{(2)}$ the particle response, A the area of focus, τ_p the pulse duration, f the repetition rate of the laser system, and S_{det} the detection efficiency (53). In HRS,

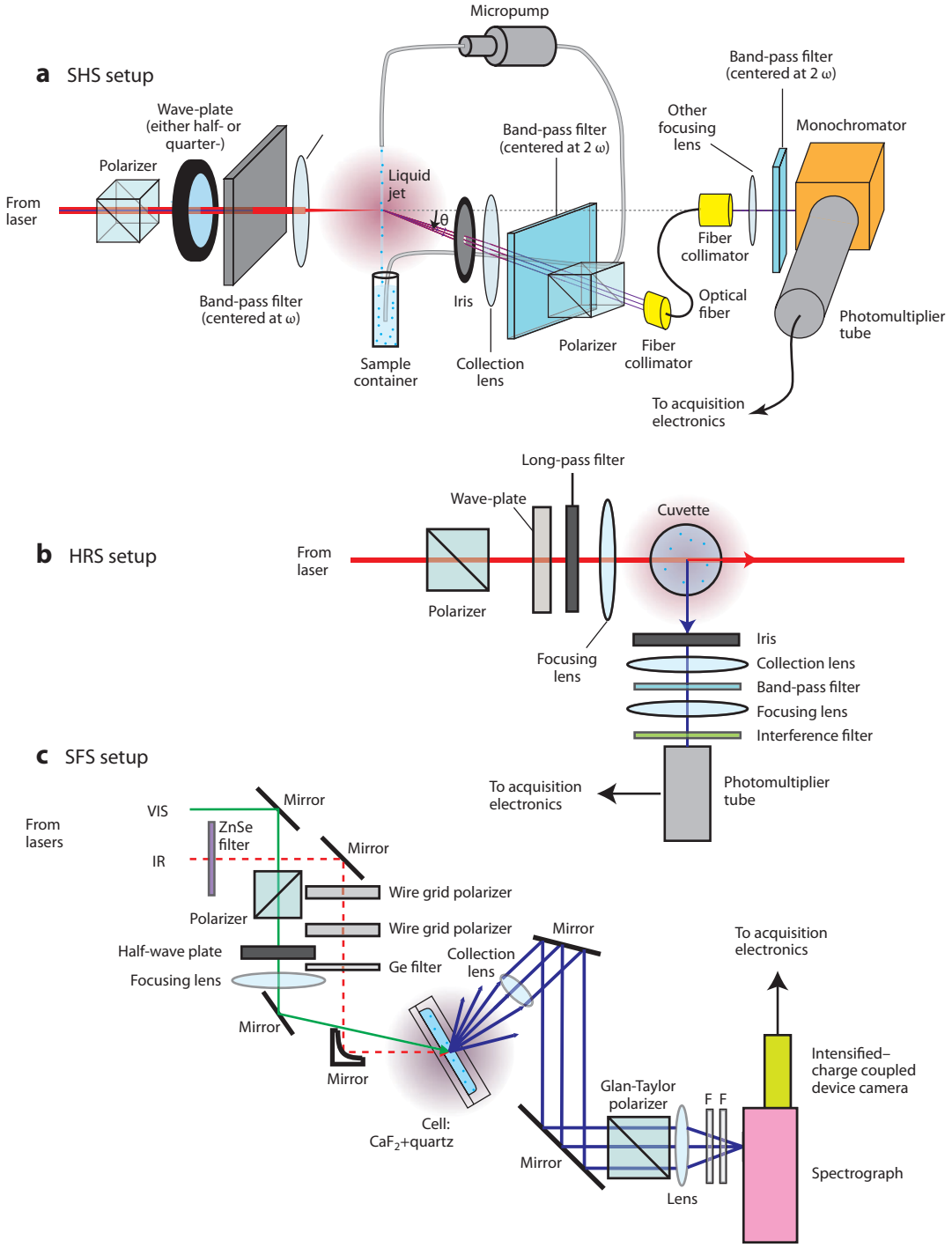

Figure 4

Schematic representation of the experimental setup to measure (*a*) second harmonic scattering (SHS), (*b*) hyper-Rayleigh scattering (HRS), and (*c*) sum frequency scattering (SFS).

SHS, and SFS, it is not a single-surface plane that is measured but rather a volume of particles in a solution.

3.1. SHS and HRS Experiments

The SHS experiments are usually performed using the output of a femtosecond Ti:sapphire laser whose output is centered around 800 nm (MHz repetition rate). The light is focused in the liquid sample, and polarizers and wave plates are used to select the polarization of the fundamental. **Figure 4*a*** shows a diagram of the setup. Filters that block possible higher harmonic contributions intrinsic to the fundamental beam or generated by the optics are used to let only the fundamental reach the sample. The scattered SH photons are detected with a detection arm that contains an iris, to select the solid angle of detection of the SH signal, and a system of lenses to collimate and refocus the beam onto the detector. A monochromator and filters are used to remove (especially in the forward direction) any contributions from the fundamental. The rotation axis of the arm is centered at the overlap point of the fundamental and scattered SH beams. A polarizer can be present in the detection arm as well. For weak signals, an interference filter centered at the SH wavelength may be used instead of the monochromator. A photomultiplier tube is mounted on the arm to convert the SH intensity into a voltage value.

The sample can either be contained in a cell (as in the case of SFS) or be a liquid-jet produced in a micropump-driven flow system (54, 55); the latter system avoids any effects that might be introduced by the presence of windows.

The HRS setup is essentially an SHS setup with the detection angle fixed at 90° (**Figure 4*b***). A very important parameter in SHS, as in SFS, experiments is the density of particles in the liquid samples. Because the signal scales with the number density of particles (in the focal volume), one might think that a high density is desired. However, absorption effects need to be kept at bay and multiple scattering effects must be avoided. A compromise must be found because the optimal density depends on the size of the particle as well as the materials under study. Schneider et al. (56) used SHS to study the effect of the particle concentration on SHS from MG-adsorbed PS particles in water in the size range 0.1–2.9 μm and concluded that for each particle size, there is an optimal particle concentration to maximize the SH intensity.

3.2. SFS Experiments

SFS scattering experiments are usually performed with a pulsed femtosecond laser system. Owing to the difficulty of generating infrared pulses with enough energy, the laser system typically consists of an oscillator and one or more regenerative or chirped pulse amplifiers (57) so that enough pulse energy is available to generate infrared photons in an optical parametric generation/amplification/difference frequency generation cycle. An example of such a system can be found in Reference 58.

Just as in SHS, the overlap volume is an important parameter. Therefore, the focal volume of the infrared (IR), visible (VIS), and SF lens system must be optimized. Reference 59 contains a description of the appropriate optics. **Figure 4*c*** illustrates the SFS setup. An important difference with SHS is the need for a noncollinear geometry (as the IR and VIS beam typically need to have a different focusing optic). Also, for experiments in water, the IR beam is adsorbed by the bulk liquid. This can be circumvented by using D_2O, which has a smaller IR absorbance cross-section. As a consequence, experiments are generally performed in a smaller volume if the IR absorbance is the limiting factor. These effects as well as the dependence of the signal on the particle density and the IR power can be found in Reference 60.

For SFS, cells (*a*) should be chemically inert to the compounds in solution, (*b*) need to transmit the incoming beams, and (*c*) must have a vanishing nonlinear optical response. For the case of SFS where one infrared and one visible beam are used, the most useful material is CaF_2. In order to optimize the NLS over linear light scattering and extinction by absorbance, it is important to determine the optimum optical path length and particle density. An example of such a study can be found in Reference 60.

NLM: nonlinear Mie theory

4. PHYSICAL ORIGIN OF NONLINEAR LIGHT SCATTERING: MODELS AND EXPERIMENTS

The nonlinear optical properties of nanoparticles and microparticles have been a topic of study for many researchers. This section brings together those studies, gives an overview of the most important findings, and connects them to the general framework described in Section 2. Here, we summarize three general approaches for calculating the scattered fields.

1. **Method 1.** The first approach revolves around solving Maxwell's equations using appropriate boundary conditions (e.g., for linear or nonlinear interactions on metals or dielectrics) and source polarizations to retrieve the SH or SF field that appears at the interface. The field expression can then be evaluated for the far-field condition ($\lambda_{SF} \ll r_0$ or $R \ll |\mathbf{r}_0|$).
2. **Method 2.** The second approach uses a Green's function method in combination with the far-field approximation to find the solution for a current source derived from the polarization.
3. **Method 3.** The third approach revolves around using the principle of time reversal to evaluate the scattered field from a particle.

Each of these approaches can be used, taking into account the appropriate source (Equation 4) and approximations, which depend on the size, material, and shape of the particles.

4.1. Early Models for Metal Particles

Historically, the first modeling of nonlinear light scattering by small spheres was done in the 1980s with SHS and metal particles in mind. The motivation was the development of a set of experimental techniques to probe nanoparticle's properties. In 1982, Agarwal & Jha (61) considered the NL response of small metallic spheres as arising from the centrosymmetric bulk response:

$$\mathbf{P}^{(2)}(\mathbf{r}') = \gamma \nabla \mathbf{E}^2 + \beta\, \mathbf{E} \nabla \cdot \mathbf{E},$$

where γ and β are related to the properties of the electrons.

In 1986, Hua & Garsten (62) generalized the previous theory by calculating SHS from a small metallic sphere while considering the structure of the particles as an electronic fluid in jellium. They solved Maxwell's equations (method 1) and the hydrodynamical equation using the perturbation theory. Later, Östling et al. (63) and Dewitz et al. (64) used nonlinear Mie (NLM) theory to describe the response from small particles and cluster using a polarization induced by the surface charge.

4.2. Small Particles

NLS from isotropic particles was described by Dadap et al. (65, 66) in 1999. The scattering was described by summing up the induced polarization contributions, using the Green's function method (10) (method 2). The description was given for particles that are small compared to the wavelength, so that the **E** field across the particle can be considered as constant (the first two

leading orders of $\mathbf{k}_0\ \mathbf{r}'$ were used for the description). We refer to this method as the electrostatic approximation.

NLRGD: nonlinear Rayleigh-Gans-Debye theory

They used an augmented form of Equation 4b as a source term:

$$P_i^{(2)}(\mathbf{r}') = \chi_{S,ijk}^{(2)}(\mathbf{r}')E_j(\mathbf{r}')E_k(\mathbf{r}')\delta(r' - R) + \chi_{B,ijk}^{(2)}(\mathbf{r}')E_j(\mathbf{r}')\nabla E_k(\mathbf{r}'),$$

where S is used to indicate the surface and B the bulk contributions.

The scattering was found to originate from a dipole emission from nonlocal excitation mechanisms, arising from retardation effects of the fundamental traveling through the particle, and to a local quadrupole contribution. These two contributions have proved to be sufficient to describe the SH signal from a colloidal solution of 16-nm, spherical Ag particles in water ($k_0R = 0.25$) (34), as well as the angle-resolved (AR) signal from 55-nm ($k_0R = 0.84$) (**Figure 5*a***) and 85-nm ($k_0R = 1.30$) MG-adsorbed PS particles in water (67). Ag and Au nanoparticles in water (R = 25–50 nm; $k_0R = 0.39–0.78$) have an SH signal that varies with the polarization state of the fundamental in a way that is consistent with a nonlocal dipole and local quadrupole contribution (37, 39, 42). This shows that the small particle limit seems to be valid for larger particle size ranges than it was initially developed for $k_0R \ll 1$. The onset of an octupolar contribution is clear when the size of the Au nanoparticle is increased to R = 75 nm (68, 69). As the size of the particles becomes larger, higher multipoles will contribute to the signal as observed in the SHS pattern of micron-sized MG/PS particles in water (70, 71). Therefore, the electrostatic approximation appears to be valid when $k_0R < 1$. For larger particles, other models become appropriate.

4.3. Dielectrics with Small Refractive Index Contrast

In 1997, shortly after the first observation of surface SHS from PS particles in water, Martorell et al. (74) observed SH scattering from a colloidal crystal formed in a solution of PS particles. They calculated the SHS pattern using the Green's function approach (method 2) and the nonlinear Rayleigh-Gans-Debye (NLRGD) approximation. The NLRGD approximation considers all orders of $\mathbf{k}_0\ \mathbf{r}'$ but assumes that the fields are not distorted as they travel through the particle. Equation 4b was used as a source term. They showed that there is no scattered light in the forward direction. In 2001, Yang et al. (75) measured for the first time an AR-SHS pattern from MG adsorbed on the surface of PS particles (R = 250–500 nm; $k_0R = 3.7–7.5$) in water.

The first SFS measurements and AR scattering pattern were measured by Roke et al. (4) in 2003 from SiO_2 particles (R = 342 nm) dispersed in CCl_4 ($k_0R = 3.3$). The particles were chemically modified with a surface layer of stearyl chains. The vibrational spectrum of the alkyl chains was measured, and the AR-SFS pattern was described by NLRGD theory (method 2) adapted for noncollinear geometry and excitation with different frequencies. The AR-SFS patterns from silica particles of different sizes (R = 69, 123, 342 nm; $k_0R = 0.7, 1.2, 3.3$) were measured as well, and the nonlinear Wentzel-Kramers-Brillioun (NLWKB) approximation, which allows for phase shift when the incoming beams travel through the particle, was introduced. Roke et al. (28) also introduced the concept of the effective particle susceptibility, which can be derived in a very simple manner using the principle of time reversal (method 3). The application of such a method makes it possible to predict the allowed and forbidden polarization combinations for different surface and bulk symmetries by considering fundamental symmetry relations, without calculating them (30).

Jen et al. (55, 70, 76) systematically studied the AR-SHS patterns generated by MG adsorbed on plain PS particles in the size range R = 25–500 nm ($k_0R = 0.4–7.5$). The authors showed how the NLRGD model fails for SHS when the particle size becomes larger than 200 nm (70). Schürer et al. have found the same for PS particles in water without adsorbed dye on the surface (77). To

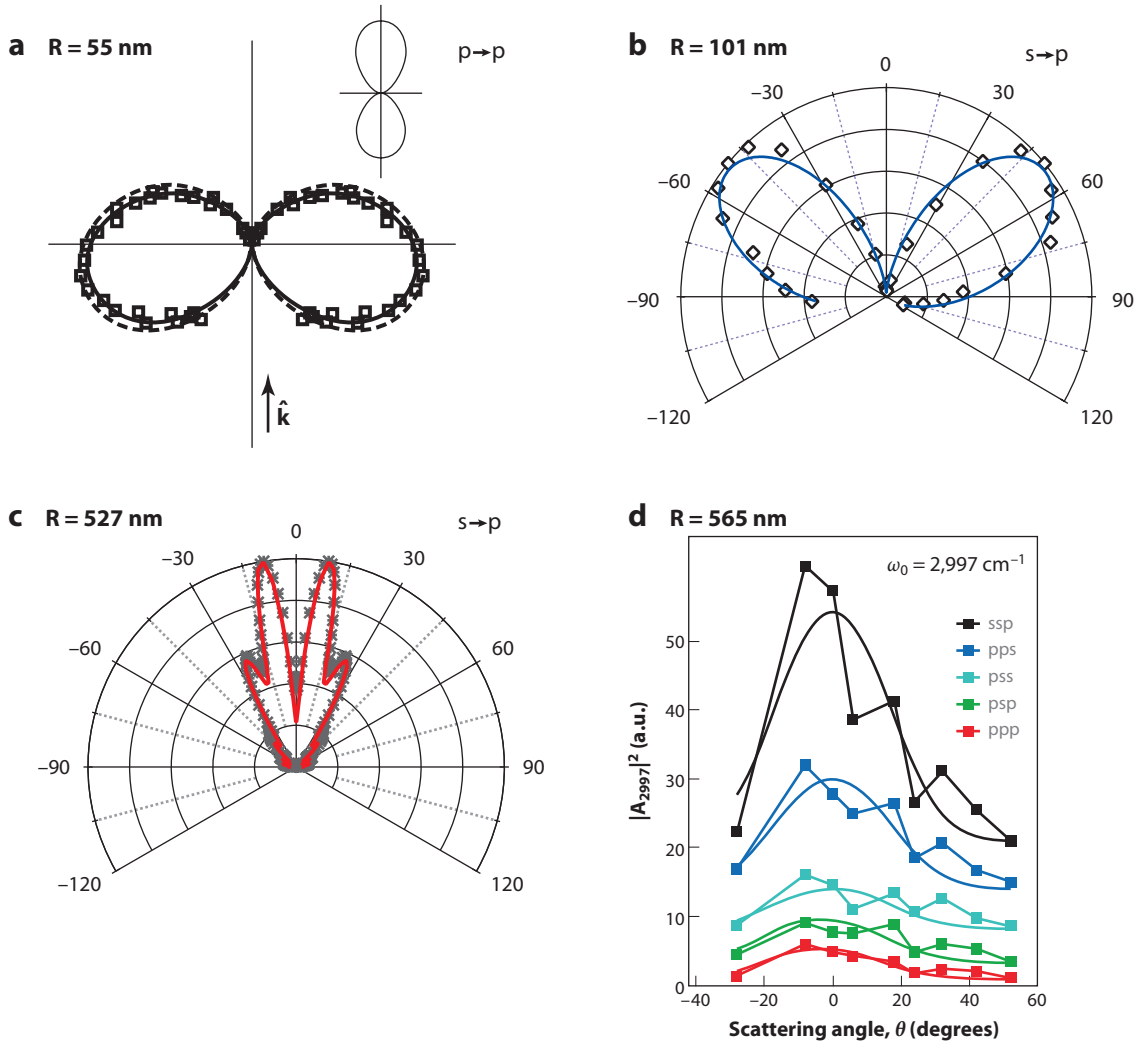

Figure 5

Angular scattering patterns in the horizontal plane for increasing values of $k_0 R$, with the angle θ defined as in **Figure 2**. The symbols represent experimental data, and the lines represent fitting curves. (*a*) SHS from a colloidal solution of MG-coated PS particles in water in p-in/p-out polarization configuration: R = 55 nm; $\lambda(\omega) = 820$ nm. The inset shows the linear scattering pattern. Adapted and reprinted with permission from Reference 67. Copyright 2006 by The American Physical Society. (*b*) SHS from a colloidal solution of MG-coated PS particles in water in s-in/p-out polarization configuration: R = 101 nm; $\lambda(\omega) = 840$ nm. Adapted and reprinted with permission from Reference 70. Copyright 2010 American Chemical Society. (*c*) Same system as in panel *b* but for a particle R = 526.5 nm. Adapted and reprinted with permission from Reference 72. Copyright 2011 by The American Physical Society. (*d*) SFS from poly(L-lactic acid) crystalline microspheres dispersed in an amorphous matrix of the same material, for different polarization configurations. The polarization combinations are indexed as SF, VIS, IR. Parameters: R = 565 nm; $\lambda_{IR} = 3{,}340$ nm; $\lambda_{VIS} = 800$ nm. This is an example of a chiral scattering pattern. Adapted and reprinted with permission from Reference 73. Copyright 2009 by The American Physical Society. The fit to the data is carried out using (*a*) SHRS theory, (*b*,*d*) NLRGD theory, and (*c*) NLM theory. Abbreviations: IR, infrared; VIS, visible; SF, sum frequency; MG, malachite green; NLM, nonlinear Mie; NLRGD, Rayleigh-Gans-Debye; p, p-polarized light; PS, polystyrene; s, s-polarized light; SHRS, second harmonic Rayleigh scattering; SHS, second harmonic scattering.

establish an exact model for scattering from spheres, NLM theory was developed for spherical particles of any kind (method 1). For SHS from dielectric particles, the NLM theory was used by Pavlyukh & Hübner (79) in 2004. Unfortunately, the authors used bulk boundary conditions. The proper boundary conditions were used already by Dadap et al. (65, 66) but they obtained the emitted field in the limit of small particles, stopping the multipole expansion at $l = 2$ (where l indicates the multipole order). In 2009, De Beer & Roke (80) developed an adapted NLM theory by using linear Mie theory (method 1) in combination with the principle of time reversal (method 3) to obtain an exact solution for the case in which the incoming beams are of different frequency and direction. This combination allows for a fast evaluation of a nonsymmetric scattering geometry and circumvents the need for nonlinear boundary conditions. Gonella & Dai (72), and Wunderlich et al. (78) have worked out the NLM theory for SHS with the correct boundary conditions (method 1). Schürer et al. were able to use the final expression to determine that $\chi^{(2)}_{\perp\perp\perp}$ is the dominant surface contribution to the SHS from the surface of PS in water (R = 100 nm; $k_0 R = 1.6$). Gonella & Dai were instead able to simultaneously fit the AR-SHS patterns from MG-adsorbed/PS particles in water (R = 25–500 nm) with the NLM theory and determine the relative weight of the different surface $\boldsymbol{\chi}^{(2)}$ components; this information led them to determine that the MG^+ molecules stand upright on the negatively charged PS surface.

Figure 5*a–c* shows examples of AR scattering patterns from PS particles with increasing size, illustrating the increased complexity of the pattern as the particle size is increased. To describe the data in **Figure 5*a***, the small particle limit (SHRS) is appropriate; for **Figure 5*b***, the NLRGD approximation suffices, whereas for the data in **Figure 5*c***, the NLM model is needed.

4.4. Nonspherical Particles

When the particles are nonspherical or aggregated, the nonlinear optical response changes dramatically. The effect of salt-induced aggregation has been studied by several groups (31, 32, 38). Dadap et al. have shown that for SFS and SHS the effects of aggregation can significantly influence a scattering experiment (13). Several groups have studied the effect of dimers and trimers on the NLS response (33, 50). Even small deviations from sphericity might induce strong changes in the optical response (37, 42, 44). Based on NLRGD theory, Dadap (81) has calculated the NLS patterns for scattering from cylinders, and De Beer et al. (29) have presented a model for calculating the nonlinear light scattering patterns of any closed surface (method 2). To show that the method works, they calculated the scattering pattern of a nano horse. They also found an elegant relationship between the form factors of linear and nonlinear scattering: If the linear scattering form factor is known, the dominant nonlinear form factor (C) can be predicted from it. To describe the SH response of particles with noncentrosymmetric shape, Bachelier et al. (82) have used a finite element method (method 2), whereas Balla et al. (83) have used a numerical, discrete dipole approximation in the small particle regime (method 2).

4.5. Chiral and Bulk Response

Nonlinear bulk scattering occurs when the particles in the bulk have a noncentrosymmetric structure. One example of this class of materials is the $P2_12_12_1$ crystal structure that occurs very often in biological structures (73). This structure gives rise to nonzero chiral tensor elements of the form $\chi^{(2)}_{\perp\parallel\parallel'}$. The chiral $\chi^{(2)}_{\perp\parallel\parallel'}$ terms give rise to chiral $\Gamma^{(2)}_{\perp\parallel\parallel'}$ terms through form factors that are different from the form factors for achiral scattering. **Figure 5*d*** shows that in the case of chiral scattering most scattered light appears in the forward direction. For chiral molecules adsorbed on the surface of a centrosymmetric particle, a scattering pattern can result, which also has the

most intensity in the forward scattering direction. The relative magnitude of the chiral surface susceptibility terms can be influenced by changing the beam geometry (30).

For centrosymmetric particles, there can be a bulk-allowed quadrupole contribution (the second term in Equation 10), which generates a scattering pattern that is indistinguishable from a surface pattern (66, 80). To distinguish between bulk quadrupole and surface contributions, Gan et al. (84) used adsorption of thiol molecules on the surface of 80-nm Ag nanoparticles at 800 nm to evaluate the surface versus bulk contribution to the SH signal. A decrease in the SH signal upon adsorption of different thiol molecules was observed at SH wavelengths close to the surface plasmon resonance. They concluded that at least 70% of the SH signal originates from the surface.

5. INTERFACE STRUCTURE AND CHEMISTRY

5.1. Molecular Conformation at Particle and Droplet Interfaces

Vibrational SFS spectra of a dispersion of small glass particles covered with chemically linked carbohydrate chains dispersed in 3 different apolar solvents (CCl_4, benzene, and hexadecane) were measured in 2005 with SFS. It was observed that the surface structure of the particles strongly depends on the type of solvent, even though the van der Waals interaction between the particles does not vary (85). The spectra were later analyzed, and the orientational distribution was extracted by analyzing polarization combinations. Also, a correlation was found between surface structure and macroscopic gelation behavior (86). de Beer & Roke (87) developed a model and software (**http://lbp.epfl.ch/**) to extract the molecular orientation of a given chemical group from SHS or SFS data using NLRGD. In this study, it was also calculated that molecular orientation shows up as most pronounced in the dominant polarization directions ssp and ppp at $qR > 1.5$. This effectively means that for particles with a radius smaller than 95 nm ($\lambda_{SF} = 400$) or 155 nm ($\lambda_{SF} = 650$), NLS spectra are not sensitive to the orientation of molecular groups. For larger particles, there is a scattering angle from which the spectral shape and polarization ratio starts to be influenced by molecular orientation. Molecular orientation can therefore be obtained most effectively and when the particles reach a certain size, as recently proved by Gonella & Dai (72) and at increasingly bigger angles as the particle size becomes smaller (87).

5.2. Metallic Nanoparticles in Liquid: Surface-Mediated Chemistry in Solution

Metallic nanoparticles have optical properties that strongly depend on the size and shape of the particle as the size of the nanoparticles is of the same order of magnitude as the electron mean free path. A very important feature of metallic nanoparticles is the presence of a surface plasmon associated with the collective oscillation of the free electrons. When the SH wavelength is resonant with such surface plasmon frequency, the signal is greatly enhanced. Because metallic nanoparticles have a large nonlinear optical response, they are used intensively for chemical sensing. Most of this work has been reviewed recently in an issue of *Chemical Reviews* devoted to plasmonics (88–95) and also in Reference 6. We therefore do not discuss any of these experiments here.

5.3. In Situ Adsorption Kinetics

Following the first observation of SHS from particle surfaces in solution (3), the PS particles-MG system in water was established as a model system for kinetic studies. MG has a large hyperpolarizability, and when the SH wavelength is tuned to the $S_2 \leftarrow S_0$ of the molecule, a large signal can be achieved. Wang et al. (54) used SHS to monitor the adsorption of methacrylate polymer on the 1-μm, sulfate-terminated PS and talc particles. Eckenrode & Dai (96) studied the adsorption

of poly-lysine on the surface of PS particles in water. The authors found that the adsorption energies are related to chain length, due to Coulombic interactions. Eckenrode et al. (97) studied the adsorption configuration of MG (positively charged) on PS with different surface terminations and concluded that MG tends to lie flat on amino-terminated PS, whereas it prefers to stand up on plain and sulfate-terminated PS. Gan et al. (98) used kinetic- and temperature-dependent SHS to obtain the rate constant for the adsorption of 1,2-benzenedithiol on 80-nm Ag nanoparticles in water as well as the adsorption energy barrier associated with the transition. Wang et al. (99) used SHS in combination with extinction and surface-enhanced Raman measurements and determined that the SHS response from stilbazolium dyes adsorbed on ~40-nm Ag nanoparticles originates from electromagnetic coupling as well as chemical binding. Haber et al. (100) followed the adsorption of MG to Au nanoparticles (16 nm) in water with SHS and found that MG adsorbs to Au nanoparticles more strongly and at higher surface densities than previously observed on PS particles or oil droplets.

5.4. Electrokinetics and Surface Potential

Yan et al. (101) used SHS to obtain the surface potential and charge of sulfate-terminated, 1-μm PS particles in water. The origin of the SH signal for charged aqueous interfaces can be attributed to three effects: (*a*) the absence of inversion symmetry at the interface, a second-order interaction, with $\chi^{(2)}$ as a source term; (*b*) DC field–aligned water molecules close to the interface; and (*c*) a $\chi^{(3)}$ process induced by three fields, i.e., the incoming beams and the DC field at the interface, so that the following term appears in Equation 4:

$$\mathbf{P} \propto \boldsymbol{\chi}^{(3)} : \mathbf{E}_1\mathbf{E}_2\mathbf{E}_{DC},$$

where $\boldsymbol{\chi}^{(3)}$ is the third-order, bulk-allowed optical susceptibility. This was originally described for planar interfaces by Ong et al. (102) and applied to scattering in 1998 (101). Liu et al. (103) used SHG spectroscopy to study the interfacial charge-transfer complex on (400-nm) TiO_2 particles in aqueous suspension. More information can be found in Reference 5.

5.5. Water

Water is the liquid of life. Investigating the properties of hydrophobic and hydrophilic interfaces is of immense importance for understanding fundamental properties of biological matter. Reviews on the vibrational properties of bulk water can be found in, e.g., Reference 104, and reviews on nonlinear optical experiments on planar water interfaces can be found in, e.g., Reference 105. Recently, nonlinear light scattering was used to get more insight into the water interface around hydrophilic or hydrophobic particles, for example, the question of how acid-base chemistry changes at an interface. Subir et al. (106) used SHS to study the protonation reaction of the carboxyl functional group fixed at the surface of PS carboxylate microspheres, with a radius of 457 nm in water. **Figure 6*a*** shows a graph of the square root of the SH signal versus the salt concentration in solution. Using Gouy-Chapman theory, the potential at the particle interface can be determined if the surface charge density is constant. If such an experiment is repeated at fixed ionic strength but as a function of pH (**Figure 6*b***), the acid-base equilibrium constant of the surface groups on the particle can be determined. The carboxyl particle surface groups are more basic compared to similar carboxylic acids in bulk aqueous medium. The shift in the acid-base equilibrium constant by a factor of four was attributed to higher surface free energy of the charged particle-liquid interface.

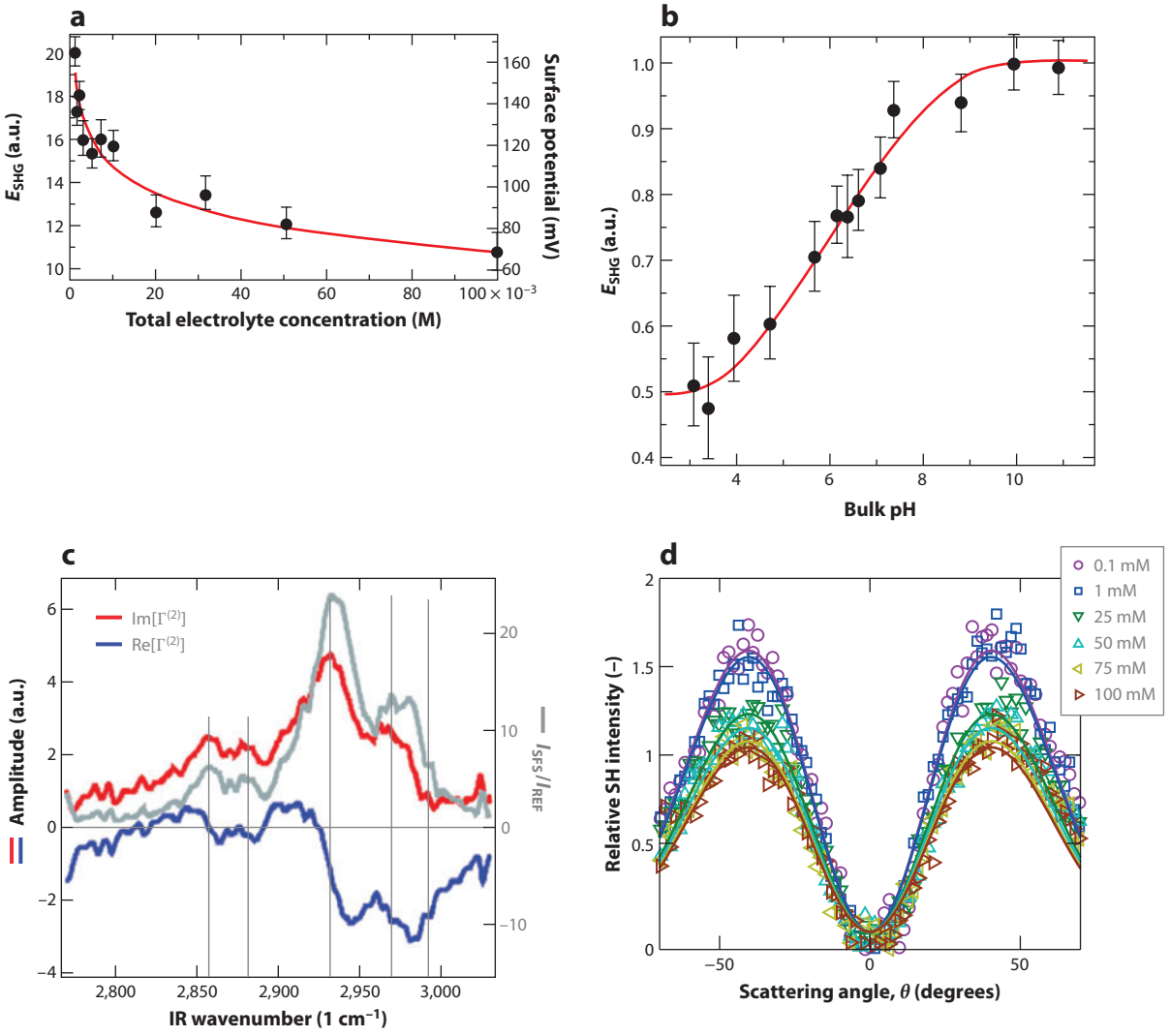

Figure 6

(*a*) SH field, E_{SHG}, as a function of bulk electrolyte concentration for the PSC colloids dispersed in water. Adapted and reprinted with permission from Reference 106. Copyright 2008 American Chemical Society. (*b*) E_{SHG} as a function of bulk pH for the PSC colloidal particles at a total ionic strength of 1 mM. Adapted and reprinted with permission from Reference 106. Copyright 2008 American Chemical Society. (*c*) Sum frequency scattering spectrum of the hydrophobic oil droplet/water interface at neutral pH (*gray curve*). The reconstructed (*blue*) real and (*red*) imaginary parts of $\mathbf{\Gamma}^{(2)}$ are also shown. Adapted and reprinted with permission from Reference 107. Copyright 2011 by the American Chemical Society. (*d*) SH scattering profiles in pp polarization configuration from charged R = 100 nm PS particles in water at different NaCl concentrations. The simulated NLM scattering profiles (*solid lines*) are scaled to fit the experimental data. Adapted and reprinted with permission from Reference 77. Copyright 2010 by the American Physical Society. Abbreviations: E_{SHG}, SH field; IR, infrared; NLM, nonlinear Mie; PS, polystyrene; PSC, polystyrene carboxylate; SH, second harmonic.

SF spectra have recently been recorded from the hydrophobic oil droplet/water interface, in combination with ζ-potential measurements. The spectrum is shown in **Figure 6*c***. The droplet ($R = 300$ nm) interface, prepared with neutral water and neutral oil, has a negative charge ($\zeta = -55$ mV). By comparing this SF spectrum, as well as the obtained imaginary and real parts of the $\boldsymbol{\Gamma}^{(2)}$ tensor, to spectra obtained from deliberately charged interfaces, it was shown that the average water orientation of a "neutral" oil/water interface is indistinguishable from the water orientation on a negatively charged interface. It is very different from a positively charged interface. Although this supports the hypothesis that the water interface is negatively charged by OH^- ions, no pH dependence was observed from a neutral bulk pH to a bulk pH of 12.5 (107).

De Beer & Roke (30) found that higher-order scattering processes have a different angular scattering pattern than second-order processes because the form factors depend on a different mathematical shape of the generated polarization. As a consequence, first-, second-, and third-order scattering will result in clearly different scattering patterns. As a useful consequence, on charged particles in aqueous systems, the surface charge effect described above emits in a different scattering pattern than a second-order-induced surface structural response (80). Schürer et al. (77) have shown that AR-SHS can be performed on bare PS particle/water interfaces. The scattering patterns as a function of ionic strength can be seen in **Figure 6*d***. This is a promising development: In the near future, it will be possible to separate $\boldsymbol{\chi}^{(2)}$ from $\boldsymbol{\chi}^{(3)}$ effects.

5.6. Droplets and Micelles

Surfactants play a very important role in the stabilization of submicron-sized oil droplets in water. Decades of research (108, 109) have been devoted to the study of surfactant behavior at planar interfaces, and the results have generally been assumed to be transferable to interfaces of small droplets. As the surface-to-volume ratio of small droplets is very different from planar interfaces, it could be asked if surfactant behavior is identical. Only few studies, and all performed in recent years, have been carried out using HRS and SHS to study micelles and emulsions. The Eisenthal group (110) was the first to use SHS to study the isothermal adsorption of MG on tetredecane oil in a water emulsion stabilized by dedecanol and sodium dodecyl sulfate (SDS). They were able to obtain from an in situ measurement the adsorption free energy and the adsorbate density of the MG molecules. The same group (101) was also able to use SHG to determine the surface electrostatic potential and surface charge density of an oil/water emulsion. More recently, Ghosh et al. (111) used HRS to determine the critical micelle concentration (CMC) based on the observation that the SH signal is different whether it is from surfactant molecules that are "free" in solution or aggregated in micelles. The Brevet group (112) investigated the interaction between probe molecules with micelles in solution by HRS: In particular they showed how the interaction of crystal violet (CV) molecules with SDS micelles can be distinguished from the interaction with freely dissolved SDS molecules. This group (23) also studied the multipolar contribution in the SH response of mixed SDS/4-(4-dihexadecylaminostyryl)-N-methylpyridinium iodide (DiA) molecular aggregates. They observed how the SH signal from DiA (cationic) molecules in solution at constant concentration is dominated by the dipolar contribution in the absence of SDS (anionic) while the quadrupolar contribution typical of spherical arrangements appears to become more important as the SDS concentration increases and SDS forms micelles of which DiA molecules are part. For very high SDS concentration, however, the number of DiA molecules per micelle is too small to reproduce a spherical arrangement, and the dipolar signal becomes dominant again. Tomalino et al. (113) instead studied the SH signal from invertible polymeric micellar structures in solvents of different polarity: The observed strong variation in the SH signal was attributed to the switching behavior of the micelles in the different solvents. They also studied the solubilization of

insoluble MG in toluene by means of amphiphilic invertible PS micelles and observed how in the beginning the SH signal increases as the MG is solubilized. The hydrophilic MG at first migrates to the micelle surface in search of a less hydrophobic environment, and this produces an increase of the signal. However, some MG molecules will get trapped by the hydrophilic fragments of the PS and transported to the interior of the micelle, producing a decrease of the signal probably related either to cancellation effects (opposite orientation of the MG molecules inside and outside the micelles) or to aggregation effects (of MG molecules in the micelle core).

Even more recently, de Aguiar et al. (114) measured the SFS response for SDS adsorbing to hexadecane oil droplets (R = 83 nm) in water by measuring the vibrational S-O stretch response in a vibrational SFS experiment. They found that the SF amplitudes change only by a factor of three when the total SDS concentration is varied from 50 μM up to the critical micelle concentration (**Figure 7*a***). Analysis showed that the interfacial density of adsorbed SDS is at least one order of magnitude lower than the interfacial density at a corresponding planar interface (4.25 nm^2 of projected surface area versus 0.46 nm^2; **Figure 7*b***). The derived maximum decrease in interfacial

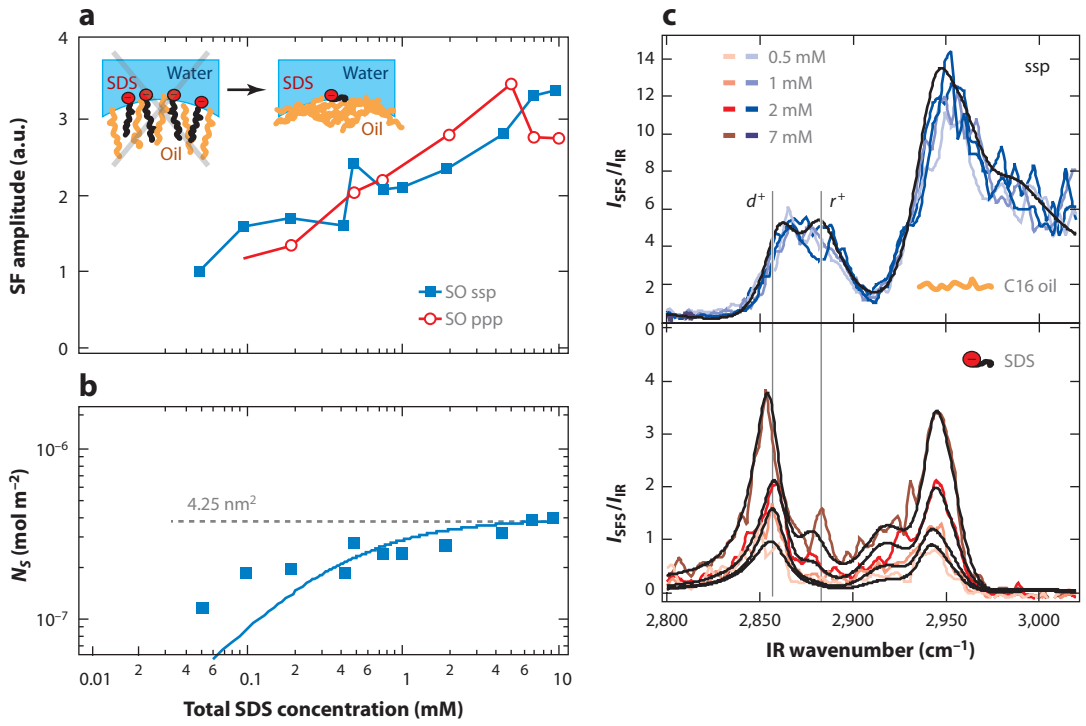

Figure 7

Surfactants at the oil droplet/water interface. (*a*) Sum frequency (SF) amplitude in ssp and ppp polarization combinations of the sulfate stretch vibrational mode at 1,070 cm^{-1}, obtained from measuring SF spectra of hexadecane droplets prepared with constant droplet size distribution and different total concentration of sodium dodecyl surfactant (SDS). The SF amplitude is proportional to the SDS surface excess (N_s). (*b*) The corresponding upper limit for N_s, derived from the amplitude data. The solid blue line is a fit to the modified Langmuir adsorption model. (*c*) Vibrational sum frequency scattering (SFS) spectra of oil molecules and surfactant molecules. It can be seen that the spectral shape of the modes of the alkyl chains in both molecules is very different, and that the oil interface spectra are not changed by the surfactants at all. The polarization combinations are indexed as SF, VIS, IR. Figure adapted and reprinted with permission from Reference 59. Copyright 2011 American Chemical Society. Abbreviations: IR, infrared; VIS, visible; SF, sum frequency; p, p-polarized light; s, s-polarized light, SDS, sodium dodecylsulfate; SO, symmetric S-O stretch mode; N_s, surface density.

tension was only 5 mN m^{-1}, much lower than the value found on planar interfaces (42 mN m^{-1}). In further SF measurements (59), the conformation of the alkyl chains of the surfactant and the oil were measured as a function of surfactant concentrations. As SDS is added to the interface, the intensity increases and the relative chain disorder changes from extremely disordered to very disordered. In contrast, the oil SF signature is not affected by the surfactant (**Figure 7*c***). de Aguiar et al. concluded, with additional experimental evidence, that oil molecules are predominantly parallel-oriented, whereas SDS appears to reside mainly on the water side, with its sulfate group interacting with water molecules.

6. BIOLOGICAL APPLICATIONS

For applications related to biology and medicine, a number of research themes have emerged over the past decade. Here, we provide a brief overview of relevant NLS and NLS-related experiments. In recent years, nonlinear microscopy has been used to image biological systems. This can be done using fluorophores, whereby the two-photon fluorescence or SHS signals are imaged (115, 116). It is also possible to use nanoparticles for imaging, and work is being done to develop nanoparticles that can link specifically to biological markers (117, 118). Reference 119 reviews nonlinear microscopy for materials research, and Reference 120 treats nonlinear microscopy in the field of biology and medicine. Another interesting development is the probing of kinetics and interfacial potentials of neurons (121, 122). The transport of ions across a bilayer leaflet can be followed with SHS (123). Furthermore, SFS has been used to measure the SF spectrum of a vesicle bilayer. Of the prepared catanionic vesicles ($R = 275$ nm), signal could be obtained from the anion head-groups, whereas the alkyl chains and the head group of the cations could not be detected (124). Although it is usually assumed that vesicle leaflets have a symmetric distribution of constituents, this seems to indicate that (thermal) fluctuations might cause the membrane structure to deviate from a completely static symmetric one.

7. CONCLUSIONS AND OUTLOOK

We have described the physical origin of incoherent and coherent NLS from particles and droplets and discussed the nonlinear optical properties of various types of systems. A cohesive overview of the more commonly used theoretical models and experimental details has been provided.

The exquisite sensitivity of NLS techniques to the interface has proved that they are formidable tools for in situ studies of solid particles and droplets in liquids. The surface/volume ratio of these systems is much higher than for their bulk counterparts, so that many new insights can be obtained about interfacial processes that are difficult to measure on planar substrates. It also allows one to perform in situ chemistry, at liquid/liquid or solid/liquid interfaces, and to study fundamental properties of emulsions, vesicles, and liposomes. Furthermore, knowing the fundamental surface structure of colloids will be a tremendous help in designing better particle systems for synthesis of soft matter tools. As an example, PS beads are used for a very large number of applications, but the orientation and density of the phenyl ring or charged groups are unknown. Other potential applications are the study of the structure of water in confined areas and the action of Hofmeister and other ions at interfaces. Also, the effect of pH and ions can be probed in much more detail.

SFS could in principle be used to track both charge density and surface potential to obtain a unique molecular picture of surface electrochemistry. Another interesting application would be tracking biomolecules by means of selective deuteration in and around model membranes in solutions (vesicles), transportation across membranes, and the working of intermembrane complexes such as ion pumps and enzymes.

DISCLOSURE STATEMENT

The authors are not aware of any affiliations, memberships, funding, or financial holdings that might be perceived as affecting the objectivity of this review.

ACKNOWLEDGMENTS

For the work related to this review, S.R. acknowledges support from the Max-Planck Society, the German Science Foundation (DFG) under contract number 560398, and the European Research Council (ERC) under contract number 240556. G.G. acknowledges the support of the U.S. Air Force Office for Scientific Research through Grant FA9550-08-1-0092 and the National Science Foundation through Grants GOALI-0616836 and CHE-1058883. G.G. also wishes to thank Prof. Hai-Lung Dai for encouragement and support.

LITERATURE CITED

1. **Terhune RW, Maker PD, Savage CM. 1965. Measurements of nonlinear light scattering. *Phys. Rev. Lett.* 14:681–84**
2. **Cyvin SJ, Rauch JE, Decius JC. 1965. Theory of hyper-Raman effects (nonlinear inelastic light scattering): selection rules and depolarization ratios for the second-order polarizability. *J. Chem. Phys.* 43:4083–95**
3. **Wang H, Yan ECY, Borguet E, Eisenthal KB. 1996. Second harmonic generation from the surface of centrosymmetric particles in bulk solution. *Chem. Phys. Lett.* 259:15–20**
4. **Roke S, Roeterdink WG, Wijnhoven JEGJ, Petukhov AV, Kleyn AW, Bonn M. 2003. Vibrational sum frequency scattering from a sub-micron suspension. *Phys. Rev. Lett.* 91:258302**
5. Eisenthal KB. 2006. Second harmonic spectroscopy of aqueous nano- and microparticle interfaces. *Chem. Rev.* 106:1462–77
6. Ray PC. 2010. Size and shape dependent second order nonlinear optical properties of nanomaterials and their application in biological and chemical sensing. *Chem. Rev.* 110:5332–65
7. Brevet P-F. 2010. Second harmonic generation in nanostructures. In *Handbook of Nanoscale Optics and Electronics*, ed. GP Wiederrecht, pp. 75–105. Amsterdam: Elsevier
8. Coulson CA, Maccoll A, Sutton LE. 1952. The polarizability of molecules in strong electric fields. *Trans. Faraday Soc.* 48:106–13
9. Feynman RP, Leighton RB, Sands ML. 1963. *The Feynman Lectures on Physics*, Vol. 1. Reading, MA: Addison-Wesley
10. Jackson JD. 1975. *Classical Electrodynamics*. New York: Wiley
11. Landau LD, Lifshitz EM. 1960. *Electrodynamics of Continuous Media*. Oxford, UK: Pergamon
12. Long DA. 2001. *The Raman Effect: A Unified Treatment of the Theory of Raman Scattering by Molecules.* New York: Wiley
13. Dadap JI, de Aguiar HB, Roke S. 2009. Nonlinear light scattering from clusters and single particles. *J. Chem. Phys.* 130:214710
14. **Bersohn R, Pao YH, Frisch HL. 1966. Double-quantum light scattering by molecules. *J. Chem. Phys.* 46:3184–98**
15. McClain WM. 1972. Polarization dependence of three-photon phenomena for randomly oriented molecules. *J. Chem. Phys.* 57:2264–72
16. Kauranen M, Persoons A. 1996. Theory of polarization measurements of second-order nonlinear light scattering. *J. Chem. Phys.* 104:3445–56
17. Hubbard SF, Petschek RG, Singer KD, D'Sidocky N, Hudson C, et al. 1998. Measurements of Kleinman-disallowed hyperpolarizability in conjugated chiral molecules. *J. Opt. Soc. Am. B* 15:289–301
18. Hubbard SF, Petschek RG, Singer KD. 1996. Spectral content and dispersion of hyper-Rayleigh scattering. *Opt. Lett.* 21:1774–76

1. First HRS observation.

2. Theory of HRS assuming Kleinman symmetry.

3. First observation of SHS from particles in liquid.

4. First SFS observation from particles in liquid.

14. General theory of HRS (no assumption of Kleinman symmetry for β).

19. Noordman OFJ, van Hulst NF. 1996. Time-resolved hyper-Rayleigh scattering: measuring first hyperpolarizabilities ß of fluorescent molecules. *Chem. Phys. Lett.* 253:145–50
20. Olbrechts G, Strobbe R, Clays K, Persoons A. 1998. High-frequency demodulation of multi-photon fluorescence in hyper-Rayleigh scattering. *Rev. Sci. Int.* 69:2223–41
21. Verbiest T, Kauranen K, Persoons A. 1994. Parametric light scattering. *J. Chem. Phys.* 101:1745–47
22. Ostroverkhov V, Petschek R, Singer KD, Sukhomlinova L, Twieg RJ, et al. 2000. Measurements of the hyperpolarizability tensor by means of hyper-Rayleigh scattering. *J. Opt. Soc. Am. B* 17:1531–42
23. Revillod G, Duboisset J, Russier-Antoine I, Benichou E, Bachelier G, et al. 2008. Multipolar contributions to the second harmonic response from mixed DiA-SDS molecular aggregates. *J. Phys. Chem. C* 112:2716–23
24. Brown F, Matsuoka M. 1969. Effect of adsorbed surface layers on second-harmonic light from silver. *Phys. Rev.* 185:985–87
25. Guyot-Sionnest P, Hunt JH, Shen YR. 1987. Sum-frequency vibrational spectroscopy of a Langmuir film: study of molecular orientation of a two-dimensional system. *Phys. Rev. Lett.* 59:1597–600
26. Harris AL, Chidsey C, Levinos N, Loiacona D. 1987. Monolayer vibrational spectroscopy by infrared-visible sum generation at metal and semiconductor surfaces. *Chem. Phys. Lett.* 141:350–56
27. Roke S. 2009. Nonlinear optical spectroscopy of soft matter interfaces. *Chem. Phys. Chem.* 10:1380–88
28. Roke S, Bonn M, Petukhov AV. 2004. Nonlinear optical scattering: the concept of the effective susceptibility. *Phys. Rev. B* 70:115106
29. de Beer AF, Roke S, Dadap JI. 2011. Theory of optical second-harmonic and sum-frequency scattering from arbitrarily shaped particles. *J. Opt. Soc. Am. B* 28:1374–84
30. de Beer AGF, Roke S. 2007. Sum frequency generation scattering from the interface of an isotropic particle: geometrical and chiral effects. *Phys. Rev. B* 75:245438
31. Vance FW, Lemon BI, Hupp JT. 1998. Enormous hyper-Rayleigh scattering from nanocrystalline gold particle suspensions. *J. Phys. Chem. B* 102:10091–93
32. Galletto P, Brevet PF, Girault HH, Antoine R, Broyer M. 1999. Enhancement of the second harmonic response by adsorbates on gold colloids: the effect of aggregation. *J. Phys. Chem. B* 103:8706–10
33. Novak JP, Brousseau LC, Vance FW, Johnson RC, Lemon BI, et al. 2000. Nonlinear optical properties of molecularly bridged gold nanoparticle arrays. *J. Am. Chem. Soc.* 122:12029–30
34. Hao EC, Schatz GC, Johnson RC, Hupp JT. 2002. Hyper-Rayleigh scattering from silver nanoparticles. *J. Chem. Phys.* 117:5963–66
35. Johnson RC, Li J, Hupp JT, Schatz GC. 2002. Hyper-Rayleigh scattering studies of silver, copper, and platinum nanoparticle suspensions. *Chem. Phys. Lett.* 356:534–40
36. Abid JP, Nappa J, Girault HH, Brevet PF. 2004. Pure surface plasmon resonance enhancement of the first hyperpolarizability of gold core-silver shell nanoparticles. *J. Chem. Phys.* 121:12577–82
37. Nappa J, Revillod G, Russier-Antoine I, Benichou E, Jonin C, Brevet PF. 2005. Electric dipole origin of the second harmonic generation of small metallic particles. *Phys. Rev. B* 71:165407
38. Das K, Uppal A, Gupta PK. 2006. Hyper-Rayleigh scattering and continuum generation of salt induced aggregates of silver nanoparticles: the effect of cation size (Li^+, Na^+ and K^+). *Chem. Phys. Lett.* 426:155–58
39. Nappa J, Russier-Antoine I, Benichou E, Jonin C, Brevet PF. 2006. Second harmonic generation from small gold metallic particles: from the dipolar to the quadrupolar response. *J. Chem. Phys.* 125:184712
40. Ray PC. 2006. Diagnostics of single base-mismatch DNA hybridization on gold nanoparticles by using the hyper-Rayleigh scattering technique. *Angew. Chem. Int. Ed.* 45:1151–54
41. Son DH, Wittenberg JS, Banin U, Alivisatos AP. 2006. Second harmonic generation and confined acoustic phonons in highly excited semiconductor nanocrystals. *J. Phys. Chem. B* 110:19884–90
42. Russier-Antoine I, Benichou E, Bachelier G, Jonin C, Brevet PF. 2007. Multipolar contributions of the second harmonic generation from silver and gold nanoparticles. *J. Phys. Chem. C* 111:9044–48
43. Darbha GK, Singh AK, Rai US, Yu E, Yu H, Chandra Ray P. 2008. Selective detection of mercury (II) ion using nonlinear optical properties of gold nanoparticles. *J. Am. Chem. Soc.* 130:8038–43
44. Russier-Antoine I, Bachelier G, Sablonière V, Duboisset J, Benichou E, et al. 2008. Surface heterogeneity in Au-Ag nanoparticles probed by hyper-Rayleigh scattering. *Phys. Rev. B* 78:035436

45. Russier-Antoine I, Huang J, Benichou E, Bachelier G, Jonin C, Brevet PF. 2008. Hyper Rayleigh scattering of protein-mediated gold nanoparticles aggregates. *Chem. Phys. Lett.* 450:345–49
46. Chandra M, Das PK. 2009. Size dependence and dispersion behavior of the first hyperpolarizability of copper nanoparticles. *Chem. Phys. Lett.* 476:62–64
47. Chandra M, Das PK. 2009. "Small-particle limit" in the second harmonic generation from noble metal nanoparticles. *Chem. Phys.* 358:203–8
48. Griffin J, Singh AK, Senapati D, Lee E, Gaylor K, et al. 2009. Sequence-specific HCV RNA quantification using the size-dependent nonlinear optical properties of gold nanoparticles. *Small* 5:839–45
49. Singh AK, Senapati D, Neely A, Kolawole G, Hawker C, Ray PC. 2009. Nonlinear optical properties of triangular silver nanomaterials. *Chem. Phys. Lett.* 481:94–98
50. Russier-Antoine I, Duboisset J, Bachelier G, Benichou E, Jonin C, et al. 2010. Symmetry cancellations in the quadratic hyperpolarizability of non-centrosymmetric gold decahedra. *J. Phys. Chem. Lett.* 1:874–80
51. Mugnier Y, Houf L, El-Kass M, Dantec RL, Hadji R, et al. 2010. In situ crystallization and growth dynamics of acentric iron iodate nanocrystals in w/o microemulsions probed by hyper-Rayleigh scattering measurements. *J. Phys. Chem. C* 115:23–30
52. Kerker M. 1969. *The Scattering of Light*. New York: Academic
53. Dadap JI, Hu X, Russell N, Ekerdt J, Lowell J, Downer M. 1995. Analysis of second-harmonic generation by unamplified, high-repetition-rate, ultrashort laser pulses at Si(001) interfaces. *IEEE J. Sel. Top. Quant.* 1:1145–55
54. Wang H, Troxler T, Yeh A, Dai H. 2000. In situ, nonlinear optical probe of surfactant adsorption on the surface of microparticles in colloids. *Langmuir* 16:2475–81
55. Jen SH, Gonella G, Dai HL. 2009. The effect of particle size in second harmonic generation from the surface of spherical colloidal particles. I. Experimental observations. *J. Phys. Chem. A* 113:4758–62
56. Schneider L, Schmid HJ, Peukert W. 2007. Influence of particle size and concentration on the second-harmonic signal generated at colloidal surfaces. *Appl. Phys. B* 87:333–39
57. Demtröder W. 2003. *Laser Spectroscopy: Basic Concepts and Instrumentation*. Berlin: Springer. 3rd ed.
58. Sugiharto AB, Johnson CM, de Aguiar HB, Aloatti L, Roke S. 2008. Generation and application of high power femtosecond pulses in the vibrational fingerprint region. *Appl. Phys. B* 91:315–18
59. de Aguiar HB, Strader ML, de Beer AGF, Roke S. 2011. Surface structure of SDS surfactant and oil at the oil-in-water droplet liquid/liquid interface: a manifestation of a non-equilibrium surface state. *J. Phys. Chem. B* 115:2970–78
60. de Aguiar HB, Samson JS, Roke S. 2011. Probing nanoscopic droplet interfaces in aqueous solution with vibrational sum-frequency scattering: a study of the effects of path length, droplet density and pulse energy. *Chem. Phys. Lett.* 512:76–80
61. Agarwal GS, Jha SS. 1982. Theory of second harmonic generation at a metal surface with surface plasmon excitation. *Solid State Commun.* 41:499–501
62. Hua XM, Gersten JI. 1986. Theory of second-harmonic generation by small metal spheres. *Phys. Rev. B* 33:3756–64
63. Östling D, Stampfli P, Bennemann K. 1993. Theory of nonlinear optical properties of small metallic spheres. *Z. Phys. D* 28:169–75
64. Dewitz JP, Hübner W, Bennemann KH. 1996. Theory for nonlinear Mie scattering from spherical metal clusters. *Z. Phys. D* 37:75–84
65. Dadap JI, Shan J, Eisenthal KB, Heinz TF. 1999. Second-harmonic Rayleigh scattering from a sphere of centrosymmetric material. *Phys. Rev. Lett.* 83:4045–48
66. Dadap JI, Shan J, Heinz TF. 2004. Theory of optical second-harmonic generation from a sphere of centrosymmetric material: small-particle limit. *J. Opt. Soc. Am. B* 21:1328–47
67. Shan J, Dadap JI, Stiopkin I, Reider GA, Heinz TF. 2006. Experimental study of optical second-harmonic scattering from spherical nanoparticles. *Phys. Rev. A* 73:023819
68. Butet J, Bachelier G, Russier-Antoine I, Jonin C, Benichou E, Brevet PF. 2010. Interference between selected dipoles and octupoles in the optical second-harmonic generation from spherical gold nanoparticles. *Phys. Rev. Lett.* 105:077401

66. Theory of SHS from a sphere of centrosymmetric material in the small-particle limit (electrostatic approximation and NLM).

69. Bachelier G, Butet J, Russier-Antoine I, Jonin C, Benichou E, Brevet P. 2010. Origin of optical second-harmonic generation in spherical gold nanoparticles: local surface and nonlocal bulk contributions. *Phys. Rev. B* 82:235403
70. Jen S, Dai H, Gonella G. 2010. The effect of particle size in second harmonic generation from the surface of spherical colloidal particles. II. The nonlinear Rayleigh-Gans-Debye model. *J. Phys. Chem. C* 114:4302–8
71. Viarbitskaya S, Kapshai V, van der Meulen P, Hansson T. 2010. Size dependence of second-harmonic generation at the surface of microspheres. *Phys. Rev. A* 81:053850

72. SH-NLM theory for particles of any size to extract information of the adsorbate orientation.

72. Gonella G, Dai HL. 2011. Determination of adsorption geometry on spherical particles from nonlinear Mie theory analysis of surface second harmonic generation. *Phys. Rev. B* 84:121402

73. de Beer AGF, de Aguiar HB, Nijsen JWF, Roke S. 2009. Detection of buried microstructures with nonlinear light scattering spectroscopy. *Phys. Rev. Lett.* 102:095502
74. Martorell J, Vilaseca R, Corbalan R. 1997. Scattering of second-harmonic light from small spherical particles ordered in a crystalline lattice. *Phys. Rev. A* 55:4520–25
75. Yang N, Angerer WE, Yodh AG. 2001. Angle-resolved second-harmonic light scattering from colloidal particles. *Phys. Rev. Lett.* 87:103902
76. Jen SH, Dai HL. 2006. Probing molecules adsorbed at the surface of nanometer colloidal particles by optical second-harmonic generation. *J. Phys. Chem. B* 110:23000–3
77. Schürer B, Wunderlich S, Sauerbeck C, Peschel U, Peukert W. 2010. Probing colloidal interfaces by angle-resolved second harmonic light scattering. *Phys. Rev. B* 82:241404
78. Wunderlich S, Schürer B, Sauerbeck C, Peukert W, Peschel U. 2011. Molecular Mie model for second harmonic generation and sum frequency generation. *Phys. Rev. B* 84:235403
79. Pavlyukh Y, Hübner W. 2004. Nonlinear Mie scattering from spherical particles. *Phys. Rev. B* 70:245434
80. de Beer AGF, Roke S. 2009. Nonlinear Mie theory for second-harmonic and sum-frequency scattering. *Phys. Rev. B* 79:155420
81. Dadap JI. 2008. Optical second-harmonic scattering from cylindrical particles. *Phys. Rev. B* 78:205322
82. Bachelier G, Russier-Antoine I, Benichou E, Jonin C, Brevet PF. 2008. Multipolar second-harmonic generation in noble metal nanoparticles. *J. Opt. Soc. Am. B* 25:955–60
83. Balla NK, So PTC, Sheppard CJR. 2010. Second harmonic scattering from small particles using discrete dipole approximation. *Opt. Expr.* 18:21603–11
84. Gan W, Gonella G, Zhang M, Dai HL. 2011. Reactions and adsorption at the surface of silver nanoparticles probed by second harmonic generation. *J. Chem. Phys.* 134:041104
85. Roke S, Buitenhuis J, van Miltenburg JC, Bonn M, van Blaaderen A. 2005. Interface-solvent effects during colloidal phase transitions. *J. Phys. Condens. Matter* 17:S3469–79
86. Roke S, Berg O, Buitenhuis J, van Blaaderen A, Bonn M. 2006. Surface molecular view of colloidal gelation. *Proc. Natl. Acad. Sci. USA* 103:13310–14

87. NLRGD model (and software) to extract the molecular orientation of a chemical group from SHS/SFS.

87. de Beer AGF, Roke S. 2010. Obtaining molecular orientation from second harmonic and sum frequency scattering experiments: angular distribution and polarization dependence. *J. Chem. Phys.* 132:234702

88. Rycenga M, Cobley CM, Zeng J, Li W, Moran CH, et al. 2011. Controlling the synthesis and assembly of silver nanostructures for plasmonic applications. *Chem. Rev.* 111:3669–712
89. Cortie MB, McDonagh AM. 2011. Synthesis and optical properties of hybrid and alloy plasmonic nanoparticles. *Chem. Rev.* 111:3713–35
90. Jones MR, Osberg KD, Macfarlane RJ, Langille MR, Mirkin CA. 2011. Templated techniques for the synthesis and assembly of plasmonic nanostructures. *Chem. Rev.* 111:3736–827
91. Mayer KM, Hafner JH. 2011. Localized surface plasmon resonance sensors. *Chem. Rev.* 111:3828–57
92. Hartland GV. 2011. Optical studies of dynamics in noble metal nanostructures. *Chem. Rev.* 111:3858–87
93. Giannini V, Fernandez-Dominguez AI, Heck SC, Maier SA. 2011. Plasmonic nanoantennas: fundamentals and their use in controlling the radiative properties of nanoemitters. *Chem. Rev.* 111:3888–912
94. Halas NJ, Lal S, Chang WS, Link S, Nordlander P. 2011. Plasmons in strongly coupled metallic nanostructures. *Chem. Rev.* 111:3913–61
95. Morton SM, Silverstein DW, Jensen L. 2011. Theoretical studies of plasmonics using electronic structure methods. *Chem. Rev.* 111:3962–94

96. Eckenrode HM, Dai HL. 2004. Nonlinear optical probe of biopolymer adsorption on colloidal particle surface: poly-L-lysine on polystyrene sulfate microspheres. *Langmuir* 20:9202–9
97. Eckenrode HM, Jen SH, Han J, Yeh AG, Dai HL. 2005. Adsorption of a cationic dye molecule on polystyrene microspheres in colloids: effect of surface charge and composition probed by second harmonic generation. *J. Phys. Chem. B* 109:4646–53
98. Gan W, Xu B, Dai HL. 2011. Activation of thiols at a silver nanoparticle surface. *Angew. Chem. Int. Ed.* 123:6752–55
99. Wang ZY, Li W, Zhou ZQ, Cui YP. 2011. Experimental indication of chemical effects in surface enhanced hyper Rayleigh scattering using dye-adsorbed Ag nanoparticles. *Optical Materials* 33:920–23
100. Haber L, Kwok SJ, Semeraro M, Eisenthal KB. 2011. Probing the colloidal gold nanoparticle/aqueous interface with second harmonic generation. *Chem. Phys. Lett.* 507:11–14
101. Yan ECY, Liu Y, Eisenthal KB. 1998. New method for determination of surface potential of microscopic particles by second harmonic generation. *J. Phys. Chem. B* 102:6331–36
102. Ong S, Zhao X, Eisenthal KB. 1992. Polarization of water molecules at a charged interface: second harmonic studies of the silica/water interface. *Chem. Phys. Lett.* 191:327–35
103. Liu Y, Dadap JI, Zimdars D, Eisenthal KB. 1999. Study of interfacial charge-transfer complex on TiO_2 particles in aqueous suspension by second-harmonic generation. *J. Phys. Chem. B* 103:2480–86
104. Bakker HJ, Skinner JL. 2010. Vibrational spectroscopy as a probe of structure and dynamics in liquid water. *Chem. Rev.* 110:1498–517
105. Shultz MJ, Schnitzer C, Simonelli D, Baldelli S. 2000. Sum frequency generation spectroscopy of the aqueous interface: ionic and soluble molecular solutions. *Int. Rev. Phys. Chem.* 19:123–53
106. Subir M, Liu J, Eisenthal KB. 2008. Protonation at the aqueous interface of polymer nanoparticles with second harmonic generation. *J. Phys. Chem. C* 112:15809–12
107. Vacha R, Rick SW, Jungwirth P, de Beer AGF, de Aguiar HB, et al. 2011. The orientation and charge of water at the hydrophobic oil droplet–water interface. *J. Am. Chem. Soc.* 133:10204–10
108. Adamson AW, Gast AP. 1997. *Physical Chemistry of Surfaces*. New York: Wiley. 6th ed.
109. Hunter RJ. 2001. *Foundations of Colloid Science*. New York: Oxford Univ. Press. 2nd ed.
110. Wang HF, Yan ECY, Liu Y, Eisenthal KB. 1998. Energetics and population of molecules at microscopic liquid and solid surfaces. *J. Phys. Chem. B* 102:4446–50
111. Ghosh S, Krishnan A, Das PK, Ramakrishnan S. 2003. Determination of critical micelle concentration by hyper-Rayleigh scattering. *J. Am. Chem. Soc.* 125:1602–6
112. Revillod G, Russier-Antoine I, Benichou E, Jonin C, Brevet P-F. 2005. Investigating the interaction of crystal violet probe molecules on sodium dodecyl sulfate micelles with hyper-Rayleigh scattering. *J. Phys. Chem. B* 109:5383–87
113. Tomalino LM, Voronov A, Kohut A, Peukert W. 2008. Study of amphiphilic polyester micelles by hyper-Rayleigh scattering: invertibility and phase transfer. *J. Phys. Chem. B* 112:6338–43
114. de Aguiar HB, de Beer AGF, Strader ML, Roke S. 2010. The interfacial tension of nanoscopic oil droplets in water is hardly affected by SDS surfactant. *J. Am. Chem. Soc.* 132:2122–23
115. Mertz J. 2004. Nonlinear microscopy: new techniques and applications. *Curr. Opin. Neurobiol.* 14:610–16
116. Baldelli S. 2008. Chemical imaging of monolayers on metal surfaces: applications in corrosion, catalysis, and self-assembled monolayers. *ChemPhysChem* 9:2291–98
117. Pu Y, Grange R, Hsieh CL, Psaltis D. 2010. Nonlinear optical properties of core-shell nanocavities for enhanced second-harmonic generation. *Phys. Rev. Lett.* 104:207402
118. Hsieh CL, Grange R, Pu Y, Psaltis D. 2010. Bioconjugation of barium titanate nanocrystals with immunoglobulin G antibody for second harmonic radiation imaging probes. *Biomaterials* 31:2272–77
119. Tong L, Chen JX. 2011. Label-free imaging through nonlinear optical signals. *Mater. Today* 14:264–73
120. Campagnola P, Dong CY. 2011. Second harmonic generation microscopy: principles and applications to disease diagnosis. *Laser Photonics Rev.* 5:13–26
121. Jiang J, Eisenthal KB, Yuste R. 2007. Second harmonic generation in neurons: electro-optic mechanism of membrane potential sensitivity. *Biophys. J.* 93:L26–28

122. Peterka D, Takahashi H, Yuste R. 2011. Imaging voltage in neurons. *Neuron* 69:9–21
123. Liu J, Subir M, Nguyen K, Eisenthal KB. 2008. Second harmonic studies of ions crossing liposome membranes in real time. *J. Phys. Chem. B* 112:15263–66
124. Strader ML, de Aguiar HB, de Beer AGF, Roke S. 2011. Direct detection of vesicle bilayer asymmetry in catanionic vesicles using vibrational sum frequency scattering. *Soft Matter* 7:4959–63

Annual Review of
Physical Chemistry
Volume 63, 2012

Contents

Indexes

Errata

An online log of corrections to Annual Review of Physical Chemistry chapters (if any, 1997 to the present) may be found at http://physchem.AnnualReviews.org/errata.shtml